Third-harmonic generation in optical nanoantennas: efficiency enhancement

Zahra Razavi
Shiraz University of Technology
Hassan Pakarzadeh (pakarzadeh@sutech.ac.ir)
Shiraz University of Technology https://orcid.org/0000-0002-7561-4088
Najmeh Nozhat
Shiraz University of Technology

Research Article

Keywords: optical nanoantennas, Third-Harmonic Generation (THG), output spectrum, dipole and bowtie structures

Posted Date: July 12th, 2021

DOI: https://doi.org/10.21203/rs.3.rs-678900/v1

Version of Record: A version of this preprint was published at The European Physical Journal Plus on January 28th, 2022. See the published version at https://doi.org/10.1140/epjp/s13360-022-02378-3.

Third-harmonic generation in optical nanoantennas: efficiency enhancement

Zahra Razavi,[a] Hassan Pakarzadeh,[a*] Najmeh Nozhat,[b]
[a]Shiraz University of Technology, Department of Physics, Shiraz, Iran
[b]Shiraz University of Technology, Department of Electrical Engineering, Shiraz, Iran

Abstract. Optical nanoantennas have attracted a lot of research interest over the last decade owing to their unique characteristics in concentrating far-field radiation into the sub-wavelength dimensions. Also, they have been recently utilized to enhance the functionality of nonlinear optical devices. By inserting a dielectric nanoparticle within the gap of a dipole nanoantenna, the third-harmonic generation (THG) emission can be boosted. In this study, we simulate dipole and bowtie nanoantennas and compare their THG output spectra with and without the presence of indium tin oxide (ITO) nanocrystal in the nanoantennas gap. The results show that with proper design of the nanoantenna and changing the geometry from the dipole to the bowtie shape as well as inserting the ITO nanocrystal, the THG efficiency can be enhanced by a factor of three, which is higher than the dipole counterpart reported in recent established works. Our work opens a new window to generate more efficient nonlinear phenomena at nanoscale devices.

Keywords: optical nanoantennas; Third-Harmonic Generation (THG); output spectrum; dipole and bowtie structures.

***Corresponding Author's E-mail: pakarzadeh@sutech.ac.ir

1 Introduction

Dipole and bowtie nanoantennas (BNAs) have been used recently in many researches [1-3]. Localized field enhancement and spatial confinement of the incident electric field in these nanoantennas are more improved compared to the other coupled plasmon resonant-nanoparticle pair geometries [3]. One of the most important physical properties of monopole and dipole optical nanoantennas is their resonance wavelength which is substantially smaller than the free-space incident wavelength λ_0 [4,5]. Recent researches on the optical response of BNAs suggest that the sharp shape of the triangles can be considered for applications in high-resolution imaging, spectroscopy and sensing [6,7]. BNAs can localize the electromagnetic fields higher than other plasmonic nanoparticle resonance structures. Their unique geometry and high electromagnetic coupling between the two antenna arms lead to an increase in the field intensity

in the subwavelength gap. This results in an increase of nonlinear effects including second-harmonic generation (SHG) [8] and third-harmonic generation (THG) [9].

Optical nanoantennas have been recently proposed to enhance the efficiency of nonlinear optical processes such as THG which is mainly related to modifying the linear optical properties and the resonance lifetime of the plasmonic antennas[10, 11]. The confined plasmonic resonances can be identified from peaks in scattering and absorption cross-sections and near-field radiation patterns [10]. This is utilized to build optical nonlinearities at the nanoscale, without any dependency of phase-matching conditions [11]. Resonances of metallic nanoparticles like gold and silver usually take place at UV-visible wavelengths. A nanoparticle with high nonlinear characteristic used in the near field of a plasmonic structure could be beneficial for enhancing nonlinear emissions in nanoscale devices. While nonlinearity in nanophotonics have been concentrated on the inherent coupling from metallic nanostructures, a couple of works have tried to explore the coupling in nonlinear materials integrated with plasmonic devices [12]. Specifically, hybrid dielectric/plasmonic nanostructures gained a lot of interests recently for enhancing the nonlinear responses between the incident light and nanoscale components [13,14].

A hybrid plasmonic nanoantenna has been reported where the interaction of gold and indium tin oxide (ITO) was used for increasing infrared light [15,16]. It has been shown that higher THG conversion efficiency can be achieved by the hybrid crystal in comparison to its bare plasmonic arrangement. In Refs. [9] and [17] a doubled THG intensity has been observed where an ITO nanocrystal with strong third-order susceptibility has been placed in the nanoantenna gap. It is also possible to change the geometry of the optical nanoantenna or place other nonlinear

materials [18] and study the nanoantenna characteristics such as the transmission, intensity spectrum at the fundamental resonance frequency.

In this paper, we study dipole and BNAs and compare their intensity spectra with and without ITO nano-crystals inserted within the nanoantennas gap. By employing BNAs in a periodic array, we examine how the nonlinear response can be considerably changed and discuss how the enhanced near-field intensity leads to efficiency enhancement of the THG emission in the proposed hybrid BNAs. Compared with the hybrid dipole nanoantennas, we observed a noticeable increase in the output TH intensity radiated from the BNAs.

2 Theory and simulation method

To simulate our proposed nanoantenna, the three-dimensional (3D) finite-difference time-domain (FDTD) numerical method with a $1\times1\times1nm^3$ mesh in the region around the nanoantenna has been used. It is worth noting that owing to the strong coupling between neighboring nanoantennas for the array configuration, we traced the source of the nonlinear signal by extraction of figures from a single cell of the nanocrystal (isolated hybrid nanostructure). The boundary conditions for the linear and nonlinear simulations of the structure, electric and magnetic walls were set in the direction of x and y, respectively; whereas the perfectly matched layers (PMLs) boundary conditions were set along z in order to avoid numerical reflections of the incident field. Following these boundaries, an infinite array along x and y is placed over a silicon substrate which is excited by a plane-wave source polarized along x.

Palik's material data [19] is used for gold and silicon. For transmittance and reflectance, a monitor is placed at 2.5 μm above and below the silicon-gold interface, respectively, parallel to the interfaces [20]. The transmittance is obtained as a function of frequency (wavelength) using:

$$T = \int_s \mathrm{Re}\{P^m(\mathrm{f}) \cdot \mathrm{ds} \Big/ \int_s \mathrm{Re}\{P^s(\mathrm{f}) \cdot \mathrm{ds} \quad (1)$$

where $P^{m,s}$ is showing the Poynting vector at the monitor and source location, f is the frequency and S is the surface of the reference plane where the transmittance is computed. Eq. (1) was also used to calculate the reflectance R of the system by changing S to the appropriate reference plane. The absorbance is then determined as $A = 1 - T - R$.

The linear and nonlinear responses simulated at the same time in which the nonlinear investigations started by measuring the THG spectra from the hybrid and bare plasmonic nanoantenna. By having an excitation at frequency ω, the third-order susceptibility $\chi^{(3)}$ of the material induces a nonlinear polarization $P^{(3)}(3\omega)$ defined by [11]:

$$P^{(3)}(3\omega) = \varepsilon_0 \chi^3(3\omega{:}\omega\omega\omega)\,\mathrm{E}(\omega)\,\mathrm{E}(\omega)\,\mathrm{E}(\omega) \quad (2)$$

It is worth mentioning that we have numerically examined two cases where for the first case, the ITO material of the hybrid nanoantenna is considered to be linear i.e., $\chi^{(3)}_{ITO} = 0$, and for the other case is nonlinear i.e., $\chi^{(3)}_{ITO} = 2.16 \times 10^{-18}\ \frac{m^2}{V^2}$ [21], while gold is always considered nonlinear with $\chi^{(3)}_{Au} = 7.6 \times 10^{-19}\ \frac{m^2}{V^2}$ [21] and neglect the nonlinearity of the substrate.

We have simulated 40 nm-thick gold dipole nanoantenna with a 3 nm Cr adhesion layer and compared our results with the same structure consisting of two gold rods shown in Fig.1(a), with a height, a width, and a length of 40, 50, and 180 nm, respectively and also the gap distance is 20 nm. Fig. 1(b) shows the dipole nanoantenna gap filled with the ITO nano-crystal. By studying the results of Ref. [15], we have decided to change our structure to BNA with the same boundary conditions to compare our new results.

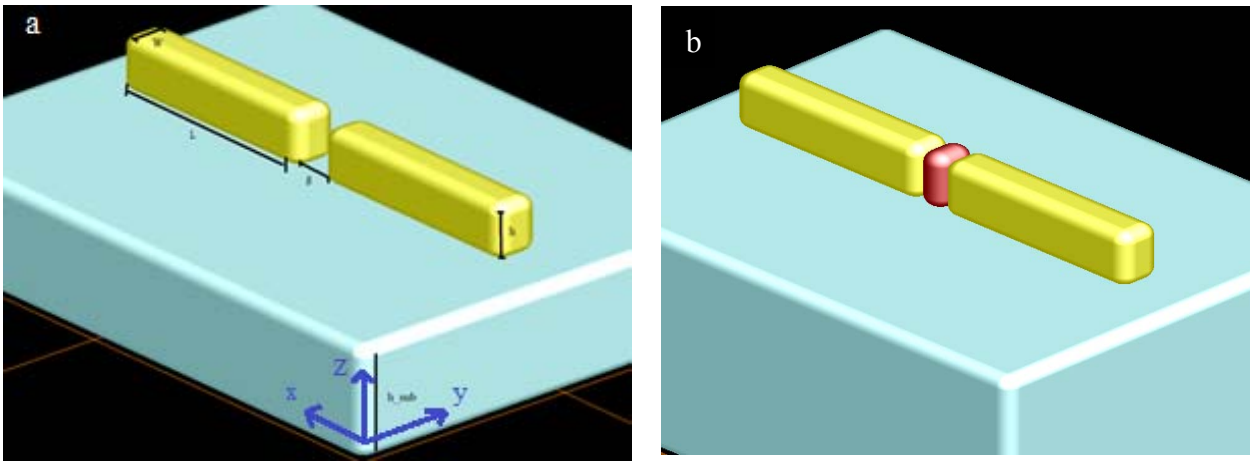

Fig. 1 (a) Geometry of the dipole nanoantenna. The polarization of the incident field is in the *x* direction as it is propagated in the *z* direction. *L*: length of the antenna; *h*: height; *g*: gap separation and (b) Dipole nanoantenna in the presence of ITO nano-crystals in nanoantenna gap.

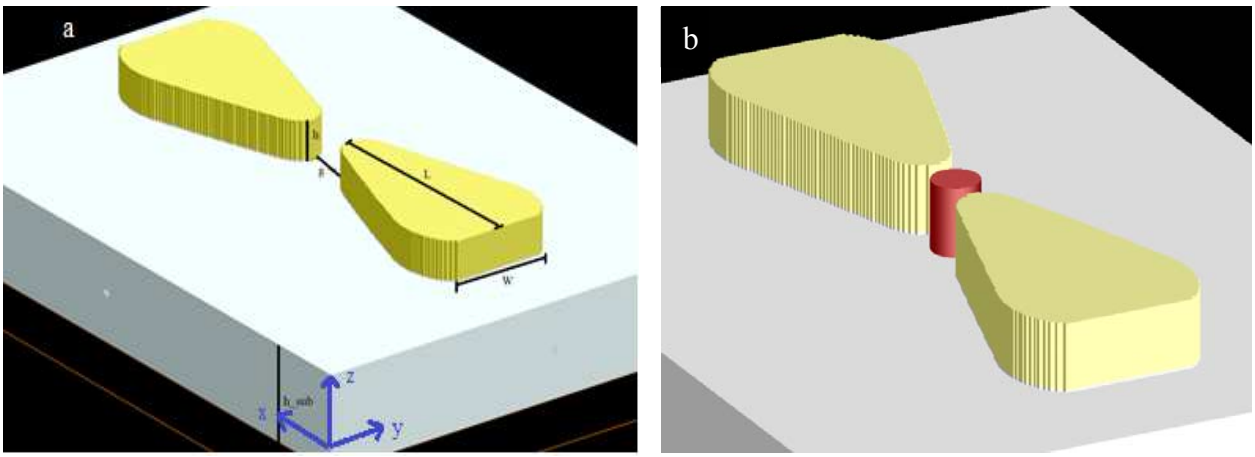

Fig. 2 (a) Geometry of the BNA. The polarization of the incident field is in the *x* direction as it is propagated in the *z* direction. *L*: length of the antenna; *h*: height; *g*: gap separation. (b) Bowtie nanoantenna in the presence of ITO nanocrystals in nanoantenna gap.

We have simulated gold BNA of 40 nm thickness with a 3 nm Cr adhesion layer with FDTD solution [22] to reach the enhanced resonance behavior of a single BNAs and their near-field intensity enhancement $|E|^2 / |E_{incident}|^2$ for our study. As the BNA resonance has a strong dependency on the polarization of the applied optical field, the incident polarization used in this simulation is parallel to the bowtie axis, which it is known as horizontal polarization. Two

equilateral triangles with 150 nm side lengths separated by a 15 nm gap has been shaped a single BNA as it is illustrated in Fig. 2(a). Also the thickness of the substrate h_{sub} is 100 nm. Fig. 2(b), shows the ITO nanocrystal which considered to be an ideal 7.5-nm-diameter cylinder, as it is located in the center of the bowtie nanoantenna gap.

3 Results and Discussion

3.1 Dipole Nanoantenna

A comparison of the linear extinction result with (incorporated with ITO) and without (bare antenna) the presence of ITO nano-crystals in the dipole nanoantenna gap is shown in Fig. 3. extinction is defined by transmission ($extinction = -\log(T)$) As it is seen, the extinction peak shifts about 75 nm towards higher wavelengths; this can be explained by changing the refractive index of the nanoantenna. In fact, the refractive index of the bare nanoantenna gap is equal to that of the air (n = 1) before adding the ITO nanocrystal while this is increased to (n = 2.9) by adding ITO nanocrystal [23]. The solid and dashed lines refer to the bare antenna and ITO incorporated within the nanoantenna gap where the fundamental resonances take place at 1050 nm and 1125 nm, respectively.

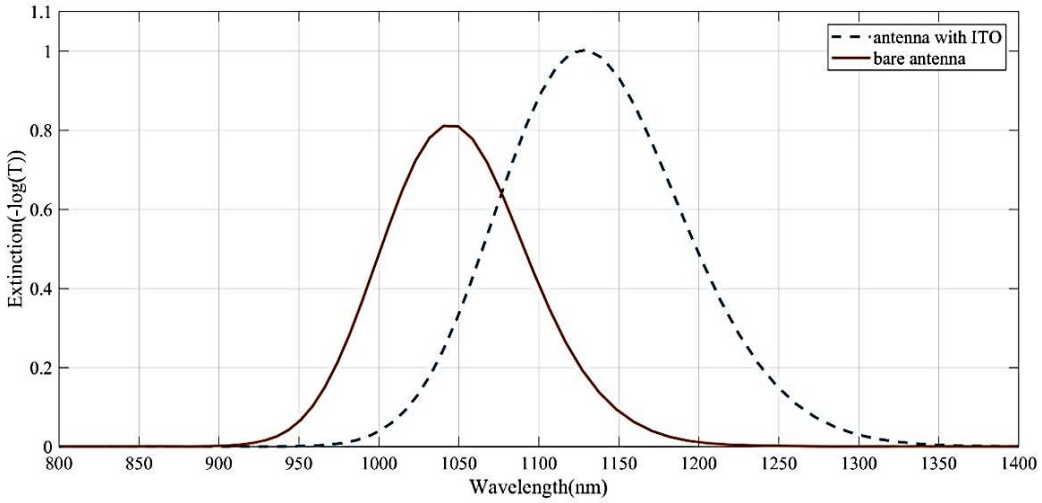

Fig. 3 Simulated extinction spectra with (dashed line) and without (solid line) the presence of ITO nanocrystal in the dipole nanoantenna gap.

The output spectrum of TH intensity for the dipole nanoantenna with ITO nanocrystal is shown in Fig. 4 which the nonlinearity of the gold and nanocrystal is considered in this study. The TH peak occurs around 380 nm, and the fundamental resonance of nanoantenna is at 1125 nm. On the other hand, when the ITO nanocrystal is inserted in the nanoantenna gap with the third-order susceptibility of $\chi_{ITO}^{(3)} = 2.16 \times 10^{-18} \frac{m^2}{V^2}$, the main resonance and the THG peaks are changed. It can be seen in Fig. 4 that the main resonance and TH peak of the structure occurs at 1125 nm and 380 nm, respectively.

In Fig. 5, we can see a comparison of the presence of ITO nanocrystal and its absence in the dipole nanoantenna gap, which shows a resonance displacement of about 30 nm due to an increase in the total refractive index of the system by adding ITO nanocrystal in its gap. Even more importantly, it is observed that the enhancement is increased about 2-fold in comparison of the THG intensity by incorporation of the ITO nanocrystals. In addition to THG, it has been

recently observed that the ITO has been found various applications in different areas such plasmon-enhanced infrared spectroscopy, nanowire network and optoelectronics [24-26].

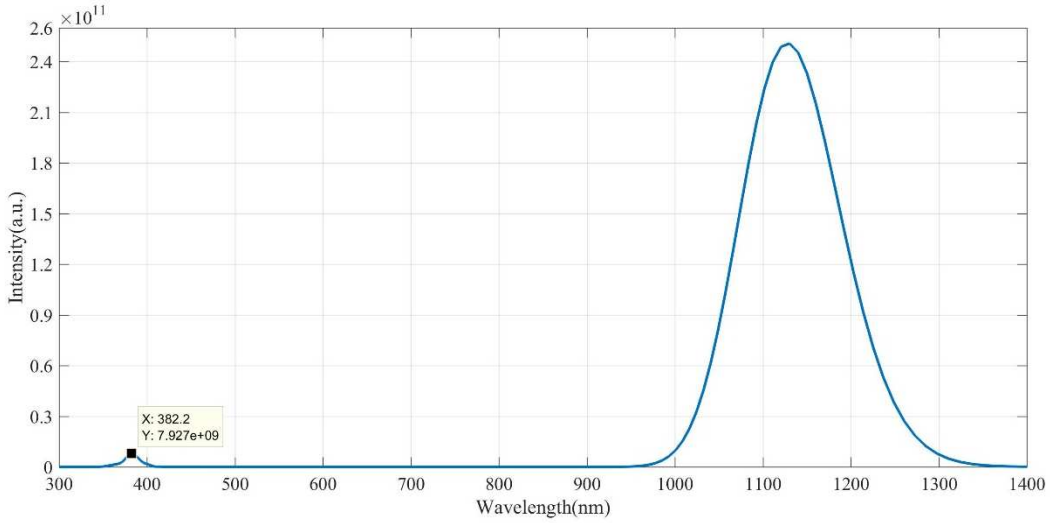

Fig. 4 Output spectrum of the dipole nanoantenna in presence of ITO nanocrystal. The THG intensity peak is shown at 382.2nm.

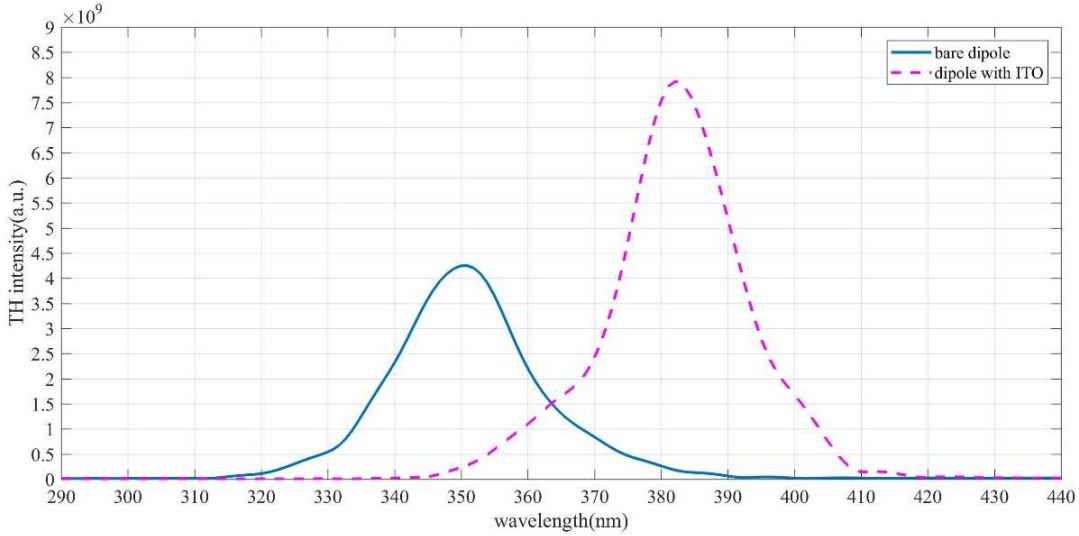

Fig. 5 Comparison of TH intensities in presence (dashed line) and absence (solid line) of ITO nanocrystal in the dipole nanoantenna.

3.2 Bowtie Nanoantenna

Now, we proceed to simulate the same boundary conditions but for the bowtie structure. The basic result of the bowtie simulation is shown in Fig. 6 so the resonance wavelength of new nanoantenna has been located around 770 nm.

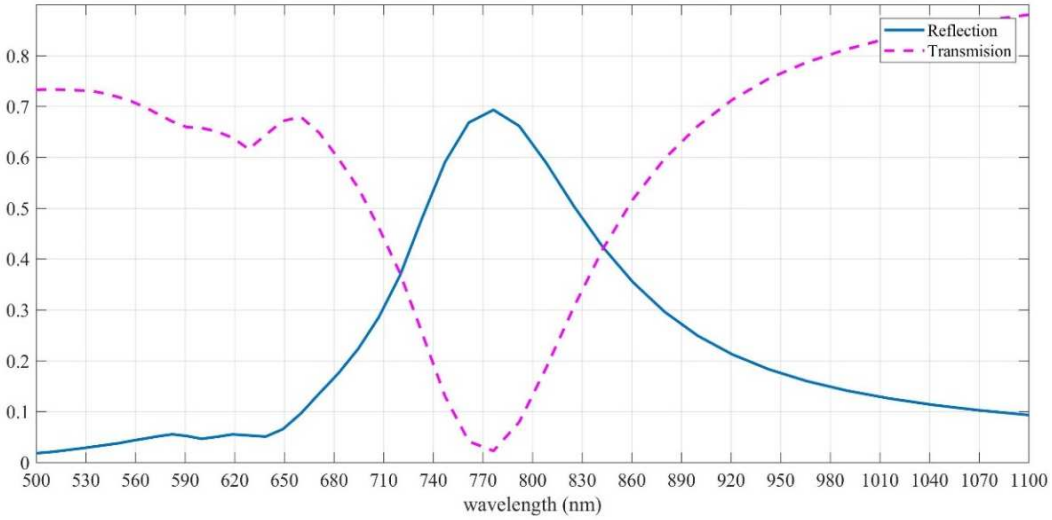

Fig. 6 Reflection and transmission spectra of the BNA.

The output spectrum of TH intensity for the bowtie nanoantenna with ITO nanocrystal is shown in Fig. 7 where the nonlinearities of the gold and nanocrystal are included in simulations. The TH peak occurs around 263 nm, and the fundamental resonance of nanoantenna is at 770 nm.

For nonlinear comparison of the dipole nanoantenna with the bowtie nanoantenna, the results of the two schemes without the presence of ITO nanocrystals are observed in the wavelength of 253 nm and the THG intensity of nanoantenna has a maximum value of 1.9×10^{10} which is shown as a blue line in Fig. 8. Also the nanoantenna resonance is increased about 20 nm with the existence of ITO nanocrystal. Furthermore, the third harmonic signal appeared at 263 nm, the maximum magnitude of the third harmonic intensity is significant, with the intensity of the third

harmonic. The state of ITO nanocrystal within the nanoantenna gap has a maximum value about 6.5×10^{10}, which in fact increased about three times greater than the bare nanoantenna.

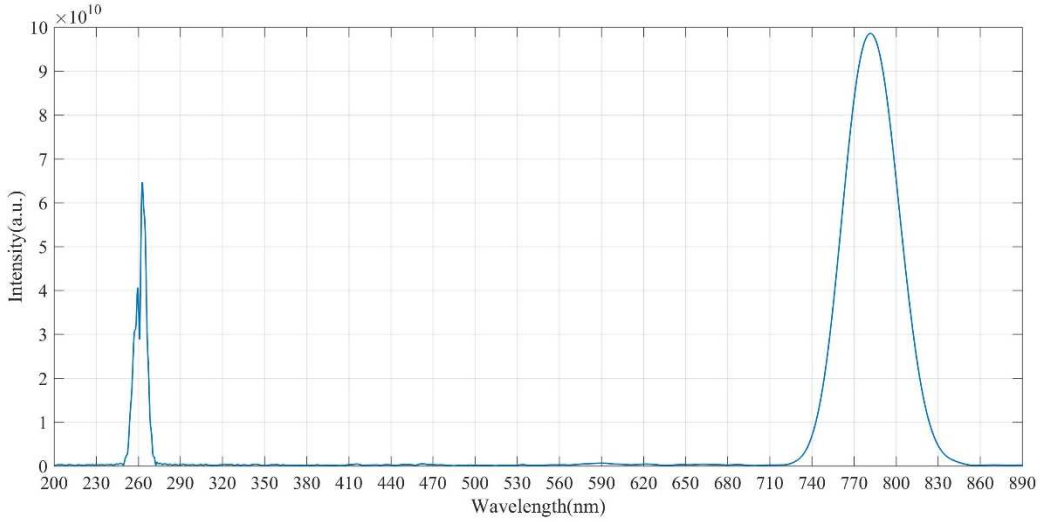

Fig. 7 Output spectrum of the BNA in presence of ITO nanocrystal. The THG intensity peak is shown at 260 nm.

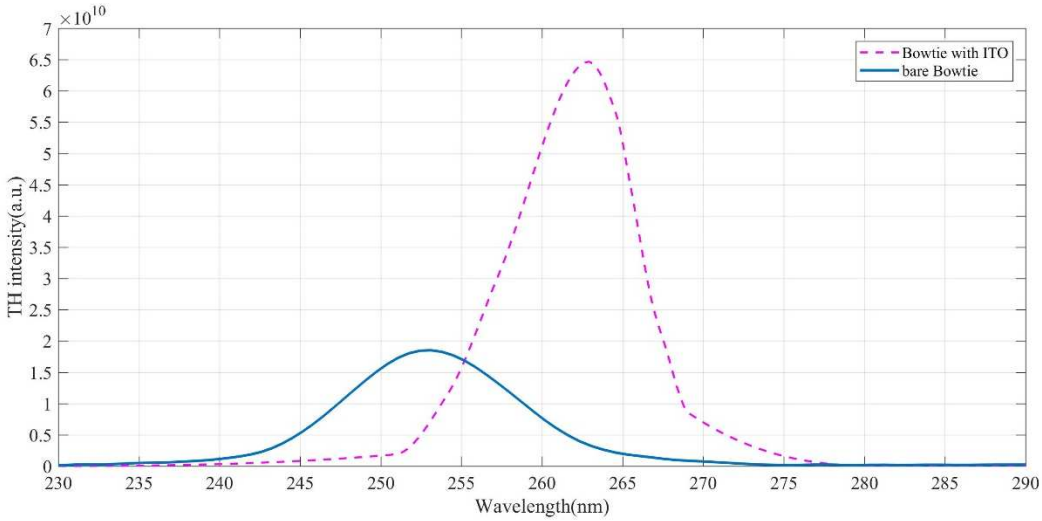

Fig. 8 Comparison of THG spectra in presence (dashed line) and absence (solid line) of ITO nanocrystal in the BNA.

The third-harmonic intensity enhancement curves for the two structures with/without the presence of ITO nanocrystal in bowtie nanoantenna are compared in Fig. 8. Notice the detection point located at the same place for two structures, which is at the center of gap between the two bowties. For a better comparison, we smooth the result of third-harmonic intensity spectrum in

Fig. 7, so we can see that the peak of the dashed red line is more than three-fold increased than the solid blue line. This means that owing to the sharp tips of the BNA structure and enhanced local fields, the THG intensity is enhanced compared with that of dipole nanoantennas.

4 Conclusion

We have simulated linear and nonlinear spectra of both dipole and bowtie nanoantennas (BNAs) and investigated the role of ITO nanocrystal when incorporated in the nanoantennas gap. It was shown that in general, the presence of ITO nanocrystal in the nanoantenna gap led to the efficiency enhancement of the THG so that in the dipole nanoantenna the enhancement factor reached twice. This is while in particular, by changing the geometry of the nanoantenna from the dipole to the bowtie structure, the enhancement factor in nonlinear mode has increased more than three-fold compared to its counterpart. Thus, our proposed BNAs with enhanced nonlinear efficiency provide new opportunities for design of tunable and sensitive nanophotonic devices for applications in nonlinear optics.

Compliance with ethical standard

Conflicts of interest: The authors declare that they have no conflicts of interest.

Availability of data and material

Data are available on request from the authors.

References

1. S. S. Mousavi, P. Berini, and D. McNamara, "Periodic plasmonic nanoantennas in a piecewise homogeneous background," *Opt. Express,* **20**(16), 18044 (2012).
2. H. Fischer and O. J. F. Martin, "Engineering the optical response of plasmonic nanoantennas," *Opt. Express*, **16**(12), 9144 (2008).

3. K. D. Ko *et al.*, "Nonlinear Optical Response from Arrays of Au Bowtie Nanoantennas," *Nano Lett.,* **11**(1), 61-65 (2011).

4. L. Novotny and N. Van Hulst, "Antennas for light," *Nat. Photonics*, **5**(2), 83–90 (2011).

5. P. Biagioni, J.-S. Huang, and B. Hecht, "Nanoantennas for visible and infrared radiation," *Rep. Prog. Phys.,* **75**(2), 024402 (2012).

6. N. Liu, M. L. Tang, M. Hentschel, H. Giessen, and A. P. Alivisatos, "Nanoantenna-enhanced gas sensing in a single tailored nanofocus," *Nat. Mater.*, **10**(8), 631–636 (2011).

7. T. Schumacher, "Optical Nanoantennas for Ultrafast Nonlinear Spectroscopy of Individual Nanosystems," PhD diss., (2014).

8. L. Ghirardini *et al.*, "Polarization properties of second-harmonic generation in AlGaAs optical nanoantennas," *Opt. Lett.*, **42**(3), 559 (2017).

9. P. Chen, C. Argyropoulos, and A. Al, "Enhanced nonlinearities using plasmonic nanoantennas," *Nanophotonics,* **1**(3-4), 221-233 (2012).

10. A. Kozbek, M. A. R. K. J. B. Loemer, and M. I. S. Calora, "Nested plasmonic resonances: extraordinary enhancement of linear and nonlinear interactions," *Opt. Express*, **25**(4), 16792–16800 (2017).

11. H. Aouani, M. Navarro-Cía, M. Rahmani, and S. A. Maier, "Unveiling the Origin of Third Harmonic Generation in Hybrid ITO-Plasmonic Crystals," *Adv. Opt. Mater.*, **3**(8), 1059–1065 (2015).

12. C. Pin, S. Ishida, G. Takahashi, K. Sudo, T. Fukaminato, and K. Sasaki, "Trapping and Deposition of Dye-Molecule Nanoparticles in the Nanogap of a Plasmonic Antenna," *ACS Omega*, **3**(5), 4878–4883 (2018).

13. G. Albrecht, M. Hentschel, S. Kaiser, and H. Giessen, "Hybrid Organic-Plasmonic Nanoantennas with Enhanced Third-Harmonic Generation," *ACS Omega*, **2**(6), 2577–2582 (2017).

14. R. Miao *et al.*, "A polarized nonlinear optical response in a topological insulator Bi 2 Se 3 –Au nanoantenna hybrid-structure for all-optical switching ," *Nanoscale*, **11**(31), pp. 14598–14606

(2019).

15. B. Metzger *et al.*, "Doubling the efficiency of third harmonic generation by positioning ITO nanocrystals into the hot-spot of plasmonic gap-antennas," *Nano Lett.*, **14**(5), 2867–2872 (2014).

16. A.C. Lesina, P. Berini and, L. Ramunno, "Origin of third harmonic generation in plasmonic nanoantennas," *Opt. Mater. Express,* **7**(5), 379–383 (2017).

17. M. Rahmani *et al.*, "Nonlinear frequency conversion in optical nanoantennas and metasurfaces: materials evolution and fabrication," *Opto-Electronic Adv.*, **1**(10), 18002101–18002112 (2018).

18. N. Weber, M. Protte, F. Walter, P. Georgi, T. Zentgraf, and C. Meier, "Double resonant plasmonic nanoantennas for efficient second harmonic generation in zinc oxide," *Phys. Rev. B*, **95**(20), 1–6 (2017).

19. Palik, Edward D., ed. *Handbook of optical constants of solids*. Vol. 3. Academic press (1998).

20. S. Amiri and N. Nozhat, "Plasmonic nanodipole antenna array with extra arms for sensing applications" *JOSA B*, **33**(8), 1769-1776 (2016).

21. S. A. Maier, H. Aouani, M. Rahmani, and M. Navarro-cı, "Third-harmonic-upconversion enhancement from a single semiconductor nanoparticle coupled to a plasmonic antenna," *Nat. Nanotechnol.,* **9**(4), 290 (2014).

22. A. C. Lesina, A. Vaccari, P. Berini, and L. Ramunno, "On the convergence and accuracy of the FDTD method for nanoplasmonics," *Opt. Express*, **23**(8), 10481 (2015).

23. Refractive index database. http://refractiveindex.info.

24. L. Galle, S. Ehrling, S. Lochmann, S. Kaskel, L. Bischoff and J. Grothe, "Conductive ITO Interfaces for Optoelectronic Applications Based on Highly Ordered Inverse Opal Thin Films," Chem.Nano. Mat., **6**, 560 (2020).

25. Z. Li, Z. Zhang, and K. Chen, "Indium–Tin–Oxide Nanostructures for Plasmon-Enhanced Infrared Spectroscopy: A Numerical Study," Micromachines,**10**, 241 (2019).

26. Li, Q., Tian, Z., Zhang, Y. et al. "3D ITO-nanowire networks as transparent electrode for all-terrain substrate," Sci. Rep. **9**, 4983 (2019).